APL Photonics

Fabrication of dense diameter-tuned quantum dot micropillar arrays for applications in photonic information processing

Cite as: APL Photonics **3**, 116103 (2018); https://doi.org/10.1063/1.5050669
Submitted: 02 August 2018 . Accepted: 12 September 2018 . Published Online: 28 September 2018

Tobias Heuser, Jan Große, Arsenty Kaganskiy, Daniel Brunner, and Stephan Reitzenstein

Fabrication of dense diameter-tuned quantum dot micropillar arrays for applications in photonic information processing

Tobias Heuser,[1] Jan Große,[1] Arsenty Kaganskiy,[1] Daniel Brunner,[2] and Stephan Reitzenstein[1,a]
[1]*Institut für Festkörperphysik, Technische Universität Berlin, Hardenbergstraße 36, D-10623 Berlin, Germany*
[2]*FEMTO-ST/Optics Department, UMR CNRS 6174, Univversité Bourgogne Franche-Comté, 15B Avenue des Montboucons, 25030 Besançon Cedex, France*

(Received 2 August 2018; accepted 12 September 2018; published online 28 September 2018)

We report on the realization of a dense, large-scale array of 900 quantum dot micropillar cavities with high spectral homogeneity. We target applications in photonic information processing such as optical reservoir computing which can be implemented in large arrays of optically coupled microlasers. To achieve the required spectral homogeneity for the underlying optical injection locking, we calculate and set the diameter of each individual micropillar within the array during the fabrication process by taking the diameter-dependent emission wavelength of the microcavities into account. Using this kind of diameter adjustment, we improve the overall wavelength homogeneity in a 30 × 30 micropillar array by 64% and reduce the standard deviation of the resonance energy distribution by 26% from 352 μeV in the planar unprocessed sample to 262 μeV in the fabricated array. In addition, we present a detailed analysis of the device quality and the diameter control of the micropillar's emission wavelength, which includes important information for the effective application of the developed fabrication method for the realization of highly homogeneous micropillar arrays in the future. https://doi.org/10.1063/1.5050669

I. INTRODUCTION

The development of high-quality quantum dot (QD) micropillar cavities has enabled numerous studies and advances in the field of cavity-enhanced nanophotonic devices. Besides the investigation of fundamental light-matter interaction in the single-QD regime of cavity quantum electrodynamics (cQED),[1,2] appealing applications of QD-micropillars include single-photon sources with close to ideal optical properties[3,4] and high-β QD-microlasers[5] showing even single-QD lasing effects.[6] More recently, the study of externally controlled QD-microlasers has led to unconventional effects such as partial injection locking in the field of nonlinear laser dynamics.[7,8] Interestingly, so far the related research has almost exclusively focused on individual QD-microcavity systems without taking advantage of coupling these devices to larger systems with enhanced functionality. For instance, network dynamics of coupled microlasers promise exciting applications in advanced photonic information processing such as neuromorphic computing.[9,10] These applications usually set stringent requirements on the fabrication of the microlasers since they rely on an extremely well-defined separation (pitch) between the individual lasers[10] and spectral homogeneity[11] within large scale laser arrays, where photonic neural networks typically require several hundred lasers[12] emitting within a frequency-range of ~50 GHz (~200 μeV).

[a]stephan.reitzenstein@physik.tu-berlin.de

The realization of spectrally homogeneous microcavity arrays is not feasible by relying upon post-fabrication tuning methods commonly applied in single-QD experiments using temperature,[2,13] magnetic field,[14,15] or the electrical field.[16,17] This issue is explained by the fact that these parameters mainly influence the emission energy of the excitonic emitters but have only minor effect, if any, on the spectral features of the cavity mode. Additionally, the tuning of individual pillars is not feasible in the case of global temperature or magnetic field tuning. Tuning of individual lasers via electrical contacts too is technologically very challenging and becomes increasingly difficult with increasing network size and density. Therefore, the spectral alignment of a large-scale network of micropillars has to be ensured already in the cavity design and fabrication process of the array, for example, by adjusting the resonance wavelength of each micropillar via its diameter. Interestingly, such "diameter-tuning" of the resonance wavelength has already been applied for individual deterministically fabricated single-QD-micropillars.[4,18] In this work, we report on the application of diameter-tuning to realize large arrays of hundreds of quantum dot micropillars with high spectral homogeneity. For this purpose, we individually tailor the resonance wavelength of single micropillars to compensate for spectral inhomogeneities of the unprocessed planar microcavity. By applying this approach, we achieve high spectral homogeneity of 262 μeV within a large-scale array of up to 900 quantum dot micropillars. Such homogeneity facilitates the interaction between the individual lasers of such arrays and allows them to form a network that can be optically injection-locked by using an external laser.[11]

II. METHOD AND SAMPLE TECHNOLOGY

The fabrication process for dense arrays of quantum dot micropillars starts with the epitaxial growth of a planar microcavity sample by means of metal-organic chemical vapor deposition (MOCVD). The layer design of the planar microcavity consists of a central one-λ thick GaAs cavity sandwiched between a lower and an upper distributed Bragg reflector (DBR) composed of 27 and 23 λ/4-thick $Al_{90}Ga_{10}As$/GaAs mirror pairs, respectively. The central GaAs cavity includes a single layer of self-assembled Stranski-Krastanow InGaAs QDs with a density of about 1×10^{10} cm^{-2}. During the growth process, the material deposition depends on the radial position of the rotating wafer which causes a radial layer thickness variation of about 2% (3 nm per DBR pair) and, in return, leads to an associated radial dependence of the cavity resonance wavelength. This typical and generally unavoidable radial variation of the resonance wavelength in the epitaxial microcavity growth is illustrated in Fig. 1(a), which shows the resonance wavelength of the planar microcavity from the center to the edge of a 2 inch wafer. For the particular sample of Fig. 1, the cavity exhibits a total radial shift of its resonance by about 25 nm. To realize homogeneous arrays of micropillar lasers, part of this resonance shift has to be compensated by adjusting the pillar diameters within the 300×300 μm^2 sample area relevant for the 30×30 micropillar array with a pitch of 10 μm chosen in this work. For this purpose, we consider the well-known relation between the micropillar diameter d_c and the resonance energy E_c of the pillar modes,[19,20]

$$E_c = \sqrt{E_0^2 + \frac{\alpha_r \hbar^2 c^2}{\varepsilon_r} \frac{4 x_{\varphi,r}^2}{d_c^2}}, \tag{1}$$

where E_0 is the position dependent resonance energy of the planar microcavity, ε_r is the effective dielectric constant of the cavity material, and $x_{\varphi,r}$ is the n_r^{th} zero of the Bessel function $J_\varphi(x)$, which has a numeric value of 2.4048 for the fundamental HE_{11} mode. We introduced the additional parameter α_r which takes the process dependent light confinement into account. It is interesting to note that there exists a trade-off between the achievable spectral compensation and the variations in the pillar emission energy induced by a given diameter accuracy. The $E_c(d_c)$ becomes steeper with decreasing diameter allowing for a larger spectral compensation. Consequently, E_c becomes more sensitive to small variations in d_c which can lead to process related spectral inhomogeneities. On the other side, this behavior allows to adjust the tuning window of this method to a given process accuracy. In practice, we can achieve a spectral compensation of about 5–8 meV in the relevant diameter range of 2–6 μm.

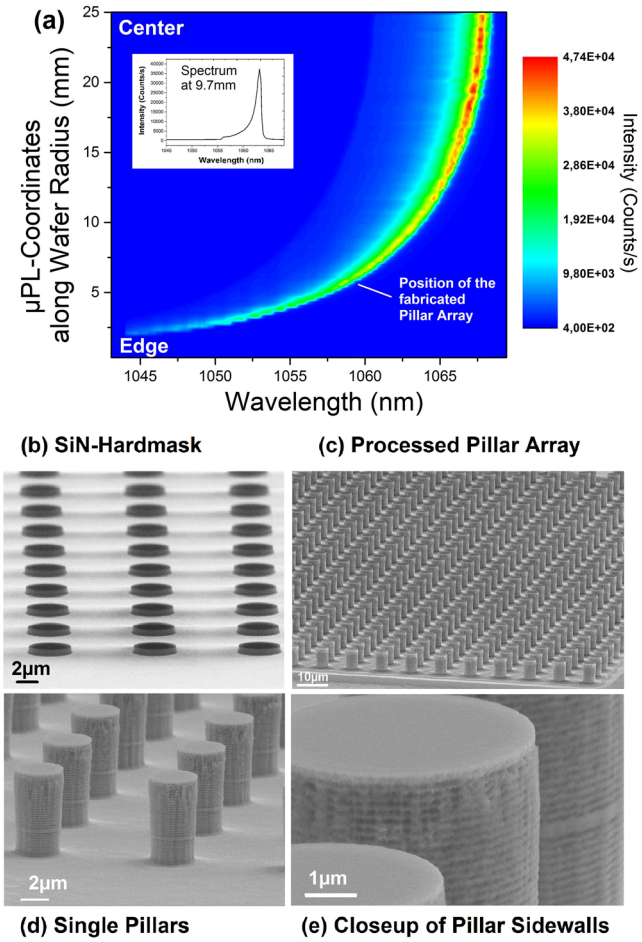

FIG. 1. (a) One dimensional μPL scan of the resonance wavelength along the radius of an unprocessed 2 in. wafer. The scan indicates a growth related radial shift of the unprocessed wafer's resonance wavelength by about 25 nm. In our nanofabrication process, this shift is compensated by precisely setting the radius of each individual QD-micropillar within a dense array during electron-beam lithography (EBL). Inset: Emission spectrum at a radial position of 9.7 mm from the edge of the wafer. [(b)–(e)] Scanning electron microscopy (SEM) images of the fabricated hard-masks and micropillar arrays with 900 resonators with a spatial pitch of about 10 μm.

To calculate the required diameter for each micropillar in the 30 × 30 array, first α_r has to be determined for the chosen etching process as we describe below. Then the resonance energy of the desired sample area needs to be mapped by micro-photoluminescence (μPL) map-scans covering the relevant area of about 300 μm × 300 μm. Here, the pitch between each pixel of the map-scans corresponds to the pitch (10 μm) of the final micropillar array so that each scanned pixel is associated with an individual pillar in the final array. To facilitate the calculation of the pillar diameters according to Eq. (1) with respect to a chosen target emission energy E_c, the measured wavelength data from the map-scans are first fitted by a polynomial function of 5th-order. The resulting calculated laser diameter pattern for the 30 × 30 pillar array is then transferred to the sample via electron-beam lithography (EBL) by using a scanning electron microscope equipped with a pattern generator. The process starts with coating of the sample with a SiN layer using plasma enhanced chemical vapor deposition (PECVD). This layer acts as material for a hard mask which ensures a high etch selectivity for the following plasma etching steps. Then the sample is coated with a negative-tone EBL-resist which is exposed using the calculated pattern of the pillar array that can be aligned with an accuracy of about 5 μm to the desired sample area. Afterward, the pattern is transferred into the 500 nm thick SiN layer by a reactive ion etching (RIE) process using a SF_6 plasma. This results in a hard mask with smooth vertical sidewalls, as illustrated in Fig. 1(b). Finally, the pillar structures

[Figs. 1(c)–1(e)] are etched by an inductively coupled plasma (ICP) RIE process using a mixed plasma recipe containing Ar_2, Cl_2, and BCl_3. The etching process by which we remove the upper DBR and up to 20 mirror pairs of the lower DBR is optimized to achieve vertical side-walls. We would like to note that process imperfections lead to (unintentional) statistical variations in the pillar diameters with a standard deviation of approximately 30 nm.

III. EXPERIMENTAL SETUP AND OPTICAL CHARACTERIZATION

Optical characterization is performed by means of high resolution μPL spectroscopy. The sample is placed onto a motorized x-y-z stage with sub-μm accuracy in all three dimensions. All measurements are performed at room temperature. Optical excitation is realized by using a diode pumped solid-state laser emitting at 671 nm which is focused via a microscope-objective (NA = 0.4) onto the surface of the sample. An additional x-y-z piezo-stage ensures spatial fine adjustment of the microscope objective. The μPL signal of the micropillar structures is then collected by using the same microscope objective and detected via a grating spectrometer with a spectral resolution of about 20 μeV, where a pinhole is used in a confocal microscope to selectively collect μPL signal from individual micropillars. The setup is automatized to record the PL emission from each individual micropillar in the 30 × 30 array. Here, the x-y-z piezo-stage is used for additional precise auto-adjustment for each individual micropillar in the array via an optical feedback-loop. This way, a spectral map is recorded in which each pixel is associated with the spectral information of a single micropillar inside the array.

We first evaluate the quality of the device fabrication by a diameter dependent optical characterization of a series of reference micropillars processed by the nominally same method as used for the micropillar arrays to be discussed below. The results are illustrated in Fig. 2, which shows a typical emission μPL spectrum (a) of a 4 μm micropillar, as well as the cavity Q-factor (b) and the fundamental resonance energy E_c (c) vs pillar diameter d_c. The 4 μm micropillar cavity shows a distinct mode spectrum with fundamental HE_{11} mode at 1.1625 eV (1066.51 nm) and a Q factor of 5450. The emission wavelength of about 1060 nm was chosen in our work to match the requirements of an existing setup for the implementation of optical reservoir computing. The diameter dependent data presented in the lower panels show the typical decrease in the Q-factors with decreasing diameter due to enhanced losses in the small diameter regime.[21] Additionally, when compared to theoretical values of about 16 000 obtained by using finite-element simulations,[22] experimental Q-factors up to 6000 at large diameters indicate absorption losses in non-ideal DBR sections and in the active area.[21] The experimental $E_c(d_c)$ dependence shows a pronounced diameter dependent blue-shift and is quantitatively described by Eq. (1). The fit yields $E_0 = 1.160\,840$ eV ± 22 μeV and $\alpha_r = 0.95 \pm 0.01$ which were used to calculate the diameter for each micropillar in the homogeneous array according to Eq. (1). It is important to note that successful diameter tuning depends sensitively on the precise knowledge of the process related parameter α_r which influences the slope of the $E_c(d_c)$ dependence in particular at low diameters. Here, α_r is a measure of the lateral light-confinement capabilities of the micropillars and increases with improved lateral light confinement. To obtain better insight into this important parameter, we numerically simulated the diameter dependent mode properties of micropillar cavities under variation of the etching depth for two different DBR compositions and slightly different resonance wavelengths using a commercial finite-element-method solver.[22] Fitting the calculated $E_c(d_c)$ dependencies allows us to determine the associated α_r parameters [see Eq. (1)] which are plotted in Fig. 2(d) vs the number of etched mirror pairs in the lower DBR for two different material compositions. As expected, α_r increases with the number of etched bottom DBR pairs because of higher lateral light confinement. On the other hand, α_r is nearly independent of the resonance wavelength and the index contrast in the DBR, which increases slightly by changing the Al content from 90% to 100% due to enhanced vertical light confinement. This result highlights that α_r is mainly influenced by the process related lateral mode confinement. For more than 10 etched mirror pairs in the lower DBR, the lateral light confinement becomes independent of the etching depth and α_r saturates. This is the regime which we use in our work.

Next we study the effect of diameter tuning on the spectral homogeneity of a processed 30 × 30 micropillar array. Figures 3 and 4 present spectroscopic results obtained for such a

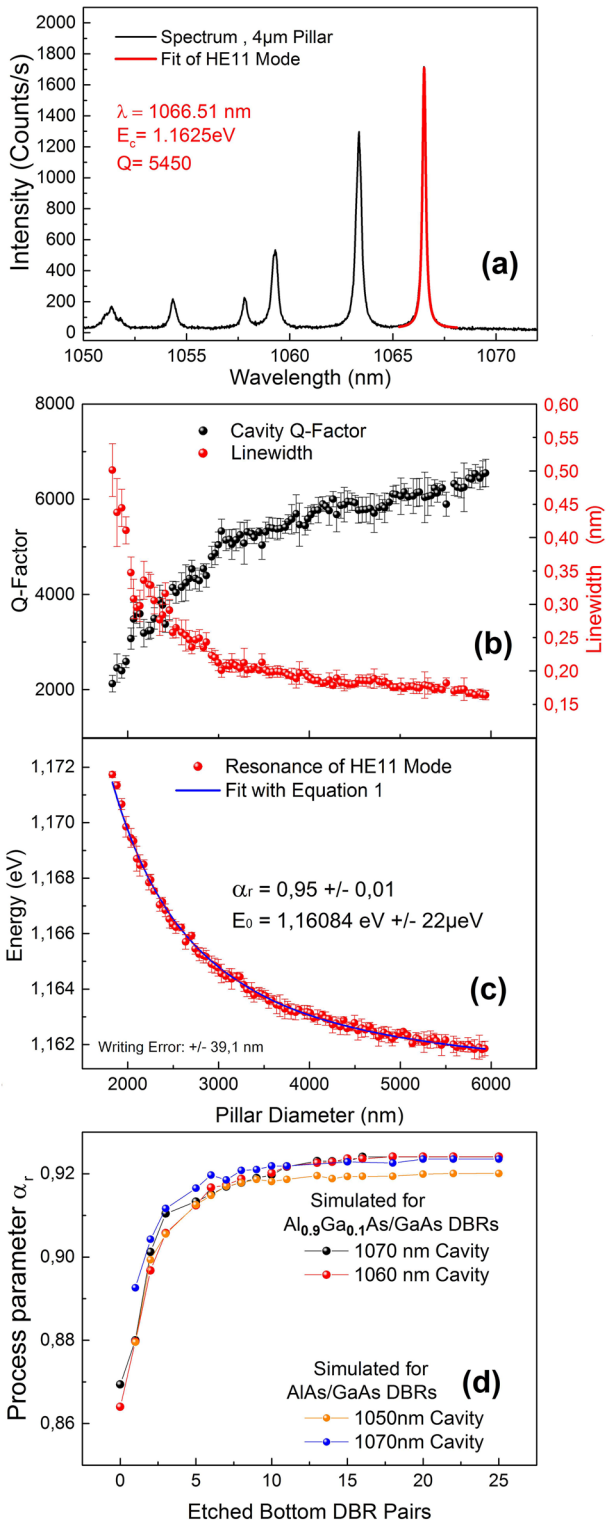

FIG. 2. (a) μPL emission spectrum of a micropillar with a diameter of 4 μm, (b) cavity Q-Factor and linewidth, and (c) resonance energy as a function of the pillar diameter. (d) Simulations of the process parameter α_r as a function of the etching depth for two different compositions ($Al_{90}Ga_{10}As$/GaAs and AlAs/GaAs) of the DBR sections and different resonance wavelengths (1050, 1060, and 1070 nm). The dependence reveals that the light confinement is reduced for low etching depths and remains almost constant for more than 10 etched bottom DBR mirror pairs, which is the regime in which we are working.

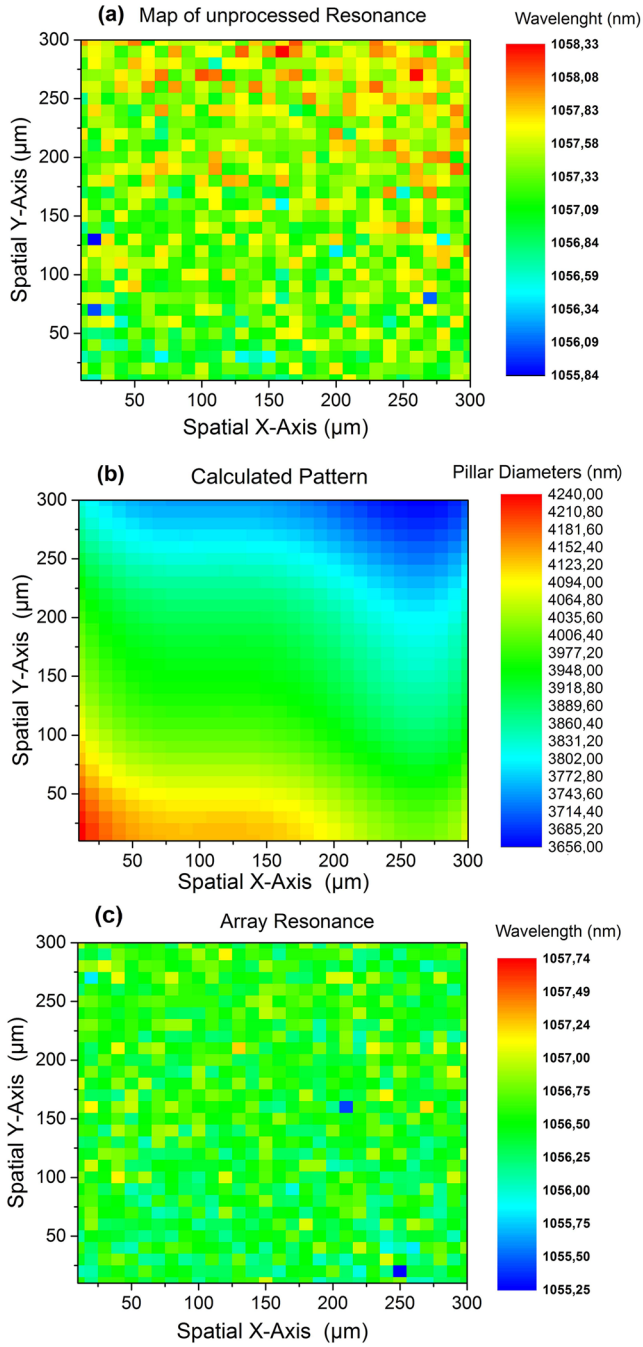

FIG. 3. μPL map-scan of the resonance wavelength of the unprocessed sample region (a) and the map of the calculated diameters for 30×30 micropillar array (b) based on the fit of the resonance wavelength shown in Fig. 4(a). (c) μPL map-scan of the HE11 resonance wavelength of the fabricated array. As the color scale shows, the wavelength trend of the unprocessed material gets compensated by the effect of the diameter tuning.

micropillar array. The array was fabricated in a sample region, marked in Fig. 1(a), with a significant radial dependence of 2.1 nm/mm of the planar cavity resonance to demonstrate the proposed concept of diameter tuning. This spectral trend is also seen in the resonance map-scan of the unprocessed material in Fig. 3(a), where the resonance wavelength decreases from the top right to the bottom left corner of the map from 1058.33 nm to 1055.84 nm. This change in the resonance is accompanied by additional growth-related local resonance fluctuations throughout the sample region resulting in

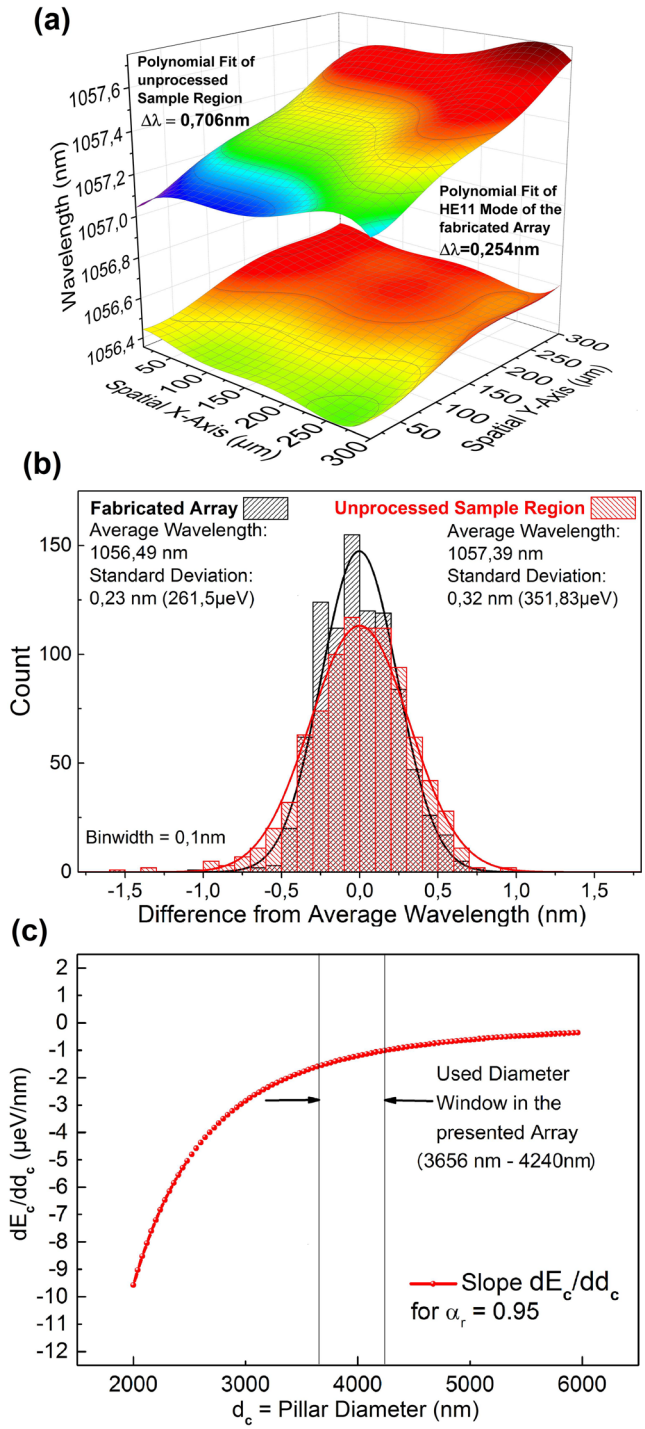

FIG. 4. (a) 2D surface plots corresponding to a polynomial fit to the μPL map-scans of the resonance wavelengths presented in Fig. 3. The plot of the unprocessed sample region has a maximum resonance wavelength difference of 0.706 nm which is reduced to 0.254 nm in the micropillar array after applying diameter tuning. (b) Histogram of the resonance wavelengths of the planar microresonator and of micropillars in the fabricated array. (c) Slope dE_c/dd_c as a function of the pillar diameter plotted for the processing parameters presented in this letter. The curve is showing the increasing influence of EBL accuracy with decreasing pillar diameter.

an average resonance wavelength of 1057.49 nm and a standard deviation of 0.32 nm (352 μeV). The diameters needed to compensate the radial resonance shift, shown in Fig. 3(b), were calculated from the polynomial fit of this spectral map which is presented in the upper panel of Fig. 4(a).

The fit also shows a maximum wavelength difference of about 0.71 nm across the chosen $300 \times 300\ \mu m^2$ sample area. This wavelength difference is smaller than the difference of the extreme values mentioned above because the fit leads effectively to an averaging of the wavelengths. In our process, the spectral inhomogeneity of the planar microcavity is compensated by a diameter variation in the range from 3656 nm to 4240 nm. Here, the large diameter regime was used to ensure that the target resonance wavelengths of the pillars are rather insensitive against process related diameter variations. The effectiveness of the diameter tuning is clearly visible in Fig. 3(c) which presents a 2D map of the fundamental (HE_{11}) mode's resonance wavelength of the fabricated array. The color scale, which covers the same wavelength range of 2.49 nm for both maps, shows that the resonance wavelength gradient is clearly reduced on the fabricated micropillar array. A quantitative comparison between the planar sample before processing (fitted data) and the fabricated micropillar array shows that the maximum resonance wavelength difference could be decreased from 0.71 nm to 0.25 nm, which means a relative reduction by 64%; see Fig. 4(a). Similarly, the standard deviation of the resonance wavelength is reduced from 0.32 nm (352 μeV) to 0.23 nm (262 μeV), which can be seen in the statistical analysis of both μPL map-scans in Fig. 4(b). As expected from the Q-factor vs diameter dependence presented in Fig. 2(a), the diameter tuning also impacts the Q-factor within the array and can become quite significant in the small diameter range. In the present case, this side effect leads to a modest Q-factor difference of about 6% between the smallest and largest micropillars in the array and is not critical for the desired application in optical reservoir computing. We would like to note that despite the overall improvement of the spectral homogeneity, local fluctuations up to 0.21 nm (230 μeV) appear in the compensated array. This value was determined by the average resonance difference between a pillar and its four nearest neighbors. The reason for this shortcoming is the fact that local resonance variations of the planar microcavity are masked by the (global) polynomial fit of the planar cavity's resonance wavelength. In future experiments, we plan to reduce the local variations by an optimized defect free epitaxial growth process and by calculating the micropillar diameter based directly on the local resonance wavelength without polynomial fitting. The latter requires a precise alignment of the processed pillar array with the scanned micropillar area by using suitable marker structures. By a suitable optimization of the reactor and the epitaxial growth process, it might become possible to almost completely suppress the radial dependence of the resonance wavelength already during sample growth. Even in this ideal case, our diameter-tuning scheme would be very beneficial to tailor the emission wavelength of the microcavities to meet the specific needs of the given applications. Considering also local variations in the resonance wavelength in the pillar-tuning process, the achievable spectral homogeneity is mainly limited by the accuracy of the EBL system used in the fabrication process. To determine the effect of diameter deviations from the calculated pattern, we calculated the slope dE_c/dd_c of the HE11 mode energy for parameters of the presented sample, which is shown in Fig. 4(c). The plot reveals that dE_c/dd_c changes in the used diameter window for this sample in a range between 1.01 and 1.59 μeV/nm. Given the mentioned writing error of our EBL system of up to 30 nm, this would lead to an achievable spectral homogeneity as low as 0.054 nm (59 μeV) for the given sample parameters, which is around a factor of 4.4 lower than the presently achieved value of 0.23 nm (262 μeV). Considering a diameter accuracy of 10 nm achievable in state-of-the-art EBL systems,[23] the spectral homogeneity could be enhanced by an additional factor of about three when using such technology in the future. In this case, it could become important to consider and compensate also the typical fundamental mode splitting on the order of a few 10 s of μeV which is related to a usually unintentional asymmetry of the pillar's cross section.[21] Finally, we would like to point out that for the application of diameter tuning, of course the spectral gradient of the wafer material which has to be compensated and the need for similar dynamical and optical properties of the individual cavities have to be considered because both factors limit the choice of available diameter tuning-window and with this the achievable compensation.

IV. SUMMARY AND CONCLUSION

In summary, we proposed and demonstrated diameter tuning as an attractive method to improve the spectral homogeneity of large scale micropillar arrays. As a spectral tuning method, we use the diameter dependence of the micropillar emission energy, which increases with decreasing pillar size

due to enhanced optical-mode confinement. We realized a 30×30 array of micropillars and present experimental results which show that the maximum resonance wavelength difference could be reduced via diameter tuning by 64% from 0.71 nm to 0.25 nm if compared to values of the unprocessed planar wafer material. Related to that, a high homogeneity in terms of the standard deviation of the fundamental mode's emission wavelength of 262 μeV (0.23 nm) was achieved. Even higher spectral homogeneity should be achievable in the future by considering not only large scale variations but also local fluctuations in the resonance wavelength of the wafer material when determining the pillar diameters for compensation. Overall, the diameter tuning method has shown promising possibilities for the realization of homogeneous, large-scale microlaser systems, for instance, for applications in optical neuromorphic computing.

ACKNOWLEDGMENTS

The research leading to these results received funding from the Volkswagen Foundation via NeuroQNet, the European Research Council under the European Union's Seventh Framework Program Grant Agreement No. 615613, and the German Research Foundation via No. CRC 787.

[1] J. Gérard, B. Sermage, B. Gayral, B. Legrand, E. Costard, and V. Thierry-Mieg, Phys. Rev. Lett. **81**, 1110 (1998).
[2] J. P. Reithmaier, G. Sek, A. Löffler, C. Hofmann, S. Kuhn, S. Reitzenstein, L. V. Keldysh, V. D. Kulakovskii, T. L. Reinecke, and A. Forchel, Nature **432**, 197 (2004).
[3] A. K. Nowak, S. L. Portalupi, V. Giesz, O. Gazzano, C. Dal Savio, P.-F. Braun, K. Karrai, C. Arnold, L. Lanco, I. Sagnes, A. Lemaître, and P. Senellart, Nat. Commun. **5**, 3240 (2014).
[4] S. Unsleber, Y.-M. He, S. Gerhardt, S. Maier, C.-Y. Lu, J.-W. Pan, N. Gregersen, M. Kamp, C. Schneider, and S. Höfling, Opt. Express **24**, 8539 (2016).
[5] M. Lermer, N. Gregersen, M. Lorke, E. Schild, P. Gold, J. Mork, C. Schneider, A. Forchel, S. Reitzenstein, S. Höfling, and M. Kamp, Appl. Phys. Lett. **102**, 052114 (2013).
[6] S. Reitzenstein, C. Böckler, A. Bazhenov, A. Gorbunov, A. Löffler, M. Kamp, V. D. Kulakovskii, and A. Forchel, Opt. Express **16**, 4848 (2008).
[7] S. André, V. Brosco, A. Shnirman, and G. Schön, Phys. Rev. A **79**, 053848 (2009).
[8] E. Schlottmann, S. Holzinger, B. Lingnau, K. Lüdge, C. Schneider, M. Kamp, S. Höfling, J. Wolters, and S. Reitzenstein, Phys. Rev. Appl. **6**, 044023 (2016).
[9] F. C. Hoppensteadt and E. M. Izhikevich, Phys. Rev. E **62**, 4010 (2000).
[10] D. Brunner and I. Fischer, Opt. Lett. **40**, 3854 (2015).
[11] J. Bueno, D. Brunner, M. Soriano, and I. Fischer, Opt. Express **25**, 2401 (2017).
[12] D. Brunner, M. C. Soriano, C. R. Mirasso, and I. Fischer, Nat. Commun. **4**, 1364 (2013).
[13] F. Brossard, X. Xu, D. Williams, M. Hadjipanayi, M. Hugues, M. Hopkinson, X. Wang, and R. Taylor, Appl. Phys. Lett. **97**, 111101 (2010).
[14] S. Reitzenstein, S. Münch, P. Franeck, A. Rahimi-Iman, A. Löffler, S. Höfling, L. Worschech, and A. Forchel, Phys. Rev. Lett. **103**, 127401 (2009).
[15] H. Kim, T. Shen, D. Sridharan, G. Solomon, and E. Waks, Appl. Phys. Lett. **98**, 091102 (2011).
[16] C. Kistner, K. Morgener, S. Reitzenstein, C. Schneider, S. Höfling, L. Worschech, A. Forchel, P. Yao, and S. Hughes, Appl. Phys. Lett. **96**, 221102 (2010).
[17] P. Munnelly, T. Heindel, A. Thoma, M. Kamp, S. Höfling, C. Schneider, and S. Reitzenstein, ACS Photonics **4**, 790 (2017).
[18] A. Dousse, L. Lanco, J. Suffczyński, E. Semenova, A. Miard, A. Lemaître, I. Sagnes, C. Roblin, J. Bloch, and P. Senellart, Phys. Rev. Lett. **101**, 267404 (2008).
[19] T. Gutbrod, M. Bayer, A. Forchel, P. A. Knipp, T. L. Reinecke, A. Tartakovskii, V. D. Kulakovskii, N. A. Gippius, and S. G. Tikhodeev, Phys. Rev. B **59**, 2223 (1999).
[20] G. Panzarini and L. C. Andreani, Phys. Rev. B **60**, 16799 (1999).
[21] S. Reitzenstein, C. Hofmann, A. Gorbunov, M. Strauß, S. H. Kwon, C. Schneider, A. Löffler, S. Höfling, M. Kamp, and A. Forchel, Appl. Phys. Lett. **90**, 251109 (2007).
[22] JCMwave GmbH, Jcmsuite version 3.12.9: Fem software package for electromagnetic waves, elasticity and heat conduction.
[23] S. Reitzenstein, N. Gregersen, C. Kistner, M. Strauss, C. Schneider, L. Pan, T. R. Nielsen, S. Höfling, J. Mork, and A. Forchel, Appl. Phys. Lett. **94**, 061108 (2009).